Mott transition in the π-flux $SU(4)$ Hubbard model on a square lattice

Zhichao Zhou,[1,2] Congjun Wu,[2] and Yu Wang[1,*]
[1]*School of Physics and Technology, Wuhan University, Wuhan 430072, China*
[2]*Department of Physics, University of California, San Diego, California 92093, USA*

(Received 23 March 2018; published 14 May 2018)

With increasing repulsive interaction, we show that a Mott transition occurs from the semimetal to the valence bond solid, accompanied by the Z_4 discrete symmetry breaking. Our simulations demonstrate the existence of a second-order phase transition, which confirms the Ginzburg-Landau analysis. The phase transition point and the critical exponent η are also estimated. To account for the effect of a π flux on the ordering in the strong-coupling regime, we analytically derive by the perturbation theory the ring-exchange term, which is the leading-order term that can reflect the difference between the π-flux and zero-flux $SU(4)$ Hubbard models.

DOI: 10.1103/PhysRevB.97.195122

I. INTRODUCTION

With the rapid development of ultracold atom experiments, the synthetic gauge field can be implemented in optical lattice systems [1–4]. Recently, the "Hofstadter butterfly" model Hamiltonian has also been achieved with ultracold atoms of ^{87}Rb [5,6]. When ultracold atoms are considered as carriers in optical lattices, they can carry large hyperfine spins. Due to the closed-shell electronic structure of alkaline-earth fermionic atoms, their hyperfine spins are simply nuclear spins, and thus the interatomic scatterings are spin-independent, leading to the $SU(2N)$ symmetry [7–11]. A series of experimental breakthroughs have been achieved with $SU(2N)$ ultracold atoms [12–16]. Interestingly, an $SU(6)$ Mott-insulating state has been observed with ^{173}Yb atoms in an optical lattice [14].

Intense curiosity has been piqued to explore the physics when high symmetry meets the synthetic gauge field. Recent theoretical studies reveal that multicomponent fermions subject to a gauge field can give rise to the spin liquid phases in the $SU(N)$ Hubbard model at the mean-field level [17] as well as in the $SU(N)$ Heisenberg model [18–20]. In solid-state physics, the $SU(2N)$ Heisenberg model was first introduced to handle strong correlation physics by employing the systematic $1/N$ expansion [21–24]. The $SU(2N)$ Heisenberg model is often considered as the low-energy effective model of the $SU(2N)$ Hubbard model at strong coupling, where the density fluctuations are neglected. It is found that the filling number of particles per site can strongly affect relevant physics of the $SU(2N)$ Heisenberg model. At quarter filling, its ground state is the long-range antiferromagnetic (AF) order on a square lattice, which is confirmed by various quantum Monte Carlo (QMC) studies [25–28]. At half-filling, different QMC methods, however, give rather conflicting results: The AF order was found to be associated with the ground state by a variational QMC simulation [29], whereas neither AF nor dimer orders exist in a projector QMC (PQMC) simulation [30].

Considering the significance of density fluctuations in a realistic fermionic system, the $SU(2N)$ Hubbard model is a prototype model for studying the interplay between density and spin degrees of freedom. Previous PQMC studies of the half-filled $SU(2)$ Hubbard model with a π flux have demonstrated a quantum phase transition from the massless Dirac semimetal phase to a Mott-insulating phase, accompanied by the appearance of long-range AF ordering [31–35]. As for the half-filled $SU(4)$ Hubbard model without a flux, with increasing Hubbard U, the AF order appears on a square lattice [36] while the valence bond solid (VBS) order emerges on a honeycomb lattice [37].

The PQMC method is basically unbiased, nonperturbative, and asymptotically correct, and particularly sign-problem-free at half filling. In this paper, we shall conduct a PQMC study of the ground-state properties of the half-filled $SU(4)$ Hubbard model with a π-flux gauge field on a square lattice, which helps to unveil novel physics that is absent in both the $SU(2)$ Hubbard model with a π flux and the $SU(4)$ Hubbard model without a flux. In the noninteracting limit, the ground state of the system is the gapless Dirac semimetal. It is shown that the increase of the Hubbard U eventually drives the system into a Mott-insulating state accompanied by VBS ordering, which breaks the Z_4 discrete symmetry. Since cubic terms are absent in the analytic part of Ginzburg-Landau (GL) free energy, the semimetal-VBS phase transition on a square lattice should be a continuous transition, in contrast to the semimetal-VBS transitions on a honeycomb lattice [37–41]. Furthermore, the critical exponent η is also extracted by finite-size scaling analysis of the numerical data.

The rest of this paper is organized as follows. In Sec. II, the model Hamiltonian and parameters of PQMC simulations are introduced. The Mott gap opening mechanism is then studied in Sec. III. Subsequently in Sec. IV, the nature of quantum phase transitions is investigated. The ring-exchange processes are analyzed in Sec. V. The conclusions are drawn in Sec. VI.

*yu.wang@whu.edu.cn

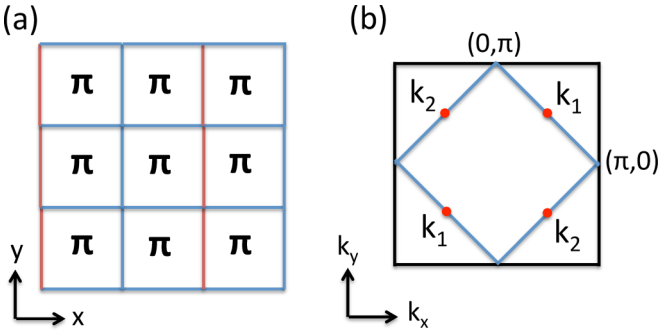

FIG. 1. (a) The hopping integrals on a square lattice. Red and blue lines correspond to $-t$ and t, respectively, hence each plaquette is penetrated by a π flux. (b) The Brillouin zone of the π-flux model on a square lattice. The blue lines depict the Fermi surface at half-filling in the absence of flux. The red points are the Dirac points at $\vec{k}_{1,2} = (\frac{\pi}{2}, \pm\frac{\pi}{2})$, and the points of $(\pm\frac{\pi}{2}, \frac{\pi}{2})$ are equivalent to $\vec{k}_{1,2}$.

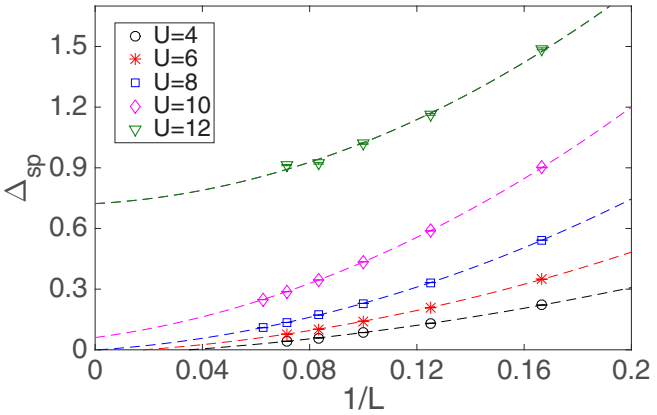

FIG. 2. The finite-size scalings of the single-particle gap Δ_{sp} for the $SU(4)$ π-flux Hubbard model as the Hubbard U varies. The quadratic polynomial fitting is used. Error bars are smaller than symbols.

II. MODEL AND METHOD

A. The $SU(4)$ π-flux Hubbard model

The $SU(4)$ Hubbard model at half-filling is defined by the lattice Hamiltonian as

$$H = -\sum_{\langle ij\rangle,\alpha} t_{ij}(c^{\dagger}_{i\alpha}c_{j\alpha} + \text{H.c.}) + \frac{U}{2}\sum_{i}(n_i - 2)^2, \qquad (1)$$

where $\langle ij\rangle$ denotes the nearest neighbors, the sum runs over sites of a square lattice, α represents spin indices running from 1 to 4, n_i is the particle number operator on site i defined as $n_i = \sum_{\alpha=1}^{4} c^{\dagger}_{i\alpha}c_{i\alpha}$ and its average value $\langle n_i\rangle = 2$ in the $SU(4)$ case, and U is the on-site repulsive interaction.

For the nearest-neighbor hopping integral t_{ij}, we use the gauge in which $t_x = t$ and $t_y = (-1)^x t$, such that the product of phases of hopping integrals around a plaquette is $e^{i\pi} = -1$, as illustrated in Fig. 1(a). At weak coupling, the low-energy effective theory of the π-flux model on a square lattice can be formulated in terms of Dirac fermions. In the weak-coupling limit of $U/t \to 0$, the dispersion relations are $\varepsilon(\vec{k}) = \pm 2t\sqrt{\cos^2(k_x) + \cos^2(k_y)}$, hence there exist eight low-energy Dirac cones located at $(\pm\frac{\pi}{2}, \pm\frac{\pi}{2})$ when taking into account the spin degeneracy, as shown in Fig. 1(b). In the atomic limit of $U/t \to \infty$, the system is in the Mott-insulating states at half filling. If a single particle is removed from one site and added to another site, the excitation energy is U, independent of the fermion components.

B. Parameters of PQMC simulations

We shall employ the zero-temperature PQMC method in the determinant formalism [42–44]. Recently, exciting progress has been made in the PQMC algorithm for the sign-problem-free simulations [45–48]. For this square-lattice $SU(4)$ Hubbard model with a π-flux gauge field, the Kramers positive decomposition guarantees the absence of a sign problem at half filling [45].

To simulate the π-flux model, the square lattice in real space is subject to the periodic boundary condition for $L = 4n$ and the antiperiodic boundary condition for $L = 4n + 2$, where n is an integer [33]. The trial wave function is chosen as the ground-state wave function of the noninteracting part of Eq. (1) with a small flux added for lifting the degeneracy at the Dirac points. The simulation parameters are set to $\Delta\tau = 0.05$ and $\beta = 40$. The measurements of physical observables are performed around $\beta/2$ after projecting onto the ground state.

III. GAP OPENING MECHANISM

In the weak-coupling regime, the system lies in the semimetal phase. With the increase of the coupling strength U, the system undergoes a phase transition from semimetal to Mott-insulating phase. In the $SU(2)$ case, this transition is well-studied via the QMC method [31–35]. In the absence of an intermediate spin-liquid phase, a second-order phase transition occurs from the Dirac semimetal phase to the AF phase. Nevertheless, the ordering of the Mott-insulating phase in the $SU(4)$ case remains unclear.

A. Single-particle gap opening

Since the Dirac cones are located at $\vec{k}_{1,2} = (\frac{\pi}{2}, \pm\frac{\pi}{2})$, we use the PQMC method to calculate the unequal-time Green's function from which the single-particle gap Δ_{sp} at $\vec{k}_{1,2}$ can be extracted for various U. Then the parameter regime of the Mott-insulating phase can be determined accordingly. By finite-size scalings we find that the critical coupling strength U_c for a single-particle gap opening lies in the range from 8 to 10, as shown in Fig. 2. This value of U_c lies in between the critical couplings of the π-flux model with $SU(2)$ symmetry and the $SU(4)$ honeycomb-lattice Hubbard model with zero flux. $U_c/t \approx 5.5$ in the former case [34,35], while $U_c/t \approx 7$ in the latter [37]. This difference can be understood with the intuitive picture as follows [37,49]. In the atomic limit $U/t \to \infty$, the single-particle gap $\Delta_{sp} = U/2$, which represents the energy barrier for adding one more fermion to the Mott-insulating background. After the hopping is switched on, the number of hopping processes is proportional to zN, which results in the bandwidth $W \approx 2zNt$. The single-particle gap can therefore

be estimated by the relation

$$\Delta_{\rm sp} \approx \frac{U}{2} - zNt, \tag{2}$$

which implies $U_c/t \approx 2zN$. Physically speaking, both the multicomponents and the increase of the coordinate number can enhance the hopping processes, which suppresses the single-particle gap $\Delta_{\rm sp}$ and thus leads to the increase of the critical coupling U_c. This argument is quantitatively consistent with our PQMC results.

B. Antiferromagnetic ordering

Generally, the equal-time $SU(2N)$ spin-spin correlation function can be defined as

$$S_{\rm spin}(i,j) = \sum_{\alpha,\beta} S_{\alpha\beta}(i) S_{\beta\alpha}(j), \tag{3}$$

where $S_{\alpha\beta}(i) = c^{\dagger}_{i,\alpha} c_{i,\beta} - \frac{\delta^{\alpha\beta}}{2N} \sum_{\gamma=1}^{2N} c^{\dagger}_{i,\gamma} c_{i,\gamma}$ are the generators of an $SU(2N)$ group obeying the commutation relation $[S_{\alpha\beta}, S_{\gamma\delta}] = \delta^{\beta\gamma} S_{\alpha\delta} - \delta^{\alpha\delta} S_{\gamma\beta}$. The spin structure factor is defined in terms of the spin-spin correlation function as follows:

$$S_{SU(2N)}(\vec{q}) = \frac{1}{L^2} \sum_{i,j} e^{i\vec{q}\cdot\vec{r}} S_{\rm spin}(i,j), \tag{4}$$

where $\vec{r}$ is the relative vector between sites i and j. Then the $SU(2N)$ long-range AF order is given by the relation

$$M = \lim_{L\to\infty} \sqrt{\frac{1}{L^2} S_{SU(2N)}(\vec{Q})} \tag{5}$$

with $\vec{Q} = (\pi,\pi)$.

Previous PQMC studies of the π-flux $SU(2)$ model [31–35] indicate that the ground state of the $SU(2)$ Mott insulator is associated with the AF order. In the zero-flux $SU(4)$ Hubbard model [36], the AF order appears starting from the weak-coupling regime, and it exhibits a nonmonotonic behavior as the interaction strength varies. It first increases with the interaction strength U, and then after reaching a maximal value at $U/t \approx 8$ it begins to be suppressed by quantum spin fluctuations as U increases further. The AF order still persists even at $U/t = 20$, while it remains unclear whether it can be suppressed to zero in the limit of $U \to \infty$.

Our simulations of the π-flux $SU(4)$ model, in contrast, demonstrate that the long-range AF order is absent in the Mott-insulating state. For our case, the finite-size scalings of the AF order parameter $M(L)$ are presented in Fig. 3. Although $M(L)$ increases with the Hubbard U, the scaling results at $L \to \infty$ show that the long-range AF order M vanishes even at $U/t = 20$. In particular, the curvatures of these $M(L)$ curves are negative, and thus it is conceivable that they converge to zero as $L \to \infty$. It is seen that both the multiflavors of fermion species and the π flux suppress the AF ordering.

C. VBS order

In this subsection, we analyze the VBS ordering pattern on a square lattice for the π-flux $SU(4)$ Hubbard model. Generally speaking, for the staggered VBS order as depicted in Fig. 4(b), its wave vector remains at (π,π) and does not break extra symmetries, hence the locations of the Dirac cones are shifted but still exist [50]. To open gaps, we shall consider the columnar VBS (cVBS) order and plaquette VBS (pVBS) order as depicted in Figs. 4(c) and 4(d), respectively. They only differ in the structure of a phase factor [51].

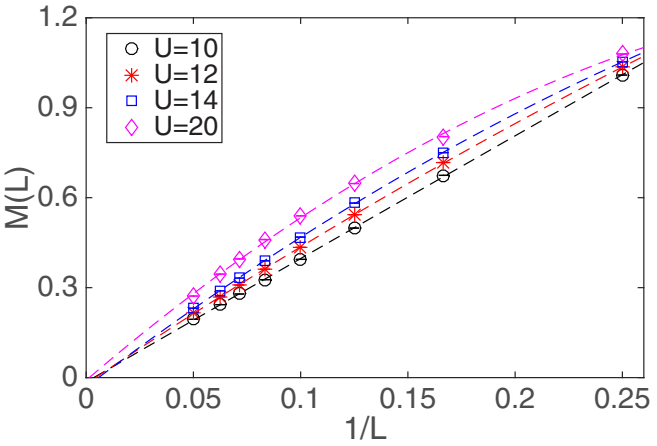

FIG. 3. Finite-size scalings of the AF order parameter $M(L)$ vs $1/L$ as U varies in the π-flux $SU(4)$ Hubbard model. The quadratic polynomial fitting is used. Error bars are smaller than symbols.

Following Ref. [51], we define a gauge-invariant VBS order below. First, the nearest-neighboring bonds $d_{i,\hat{e}_j}$ are defined via the kinetic energy:

$$d_{i,\hat{e}_j} = \frac{1}{2N} \sum_{\alpha=1}^{2N} (c^{\dagger}_{i,\alpha} t_{i,i+\hat{e}_j} c_{i+\hat{e}_j,\alpha} + \text{H.c.}), \tag{6}$$

where $\hat{e}_j$ $(j = 1,2)$ are two basis vectors of the square lattice. Then the structure factors of the VBS along the x and y

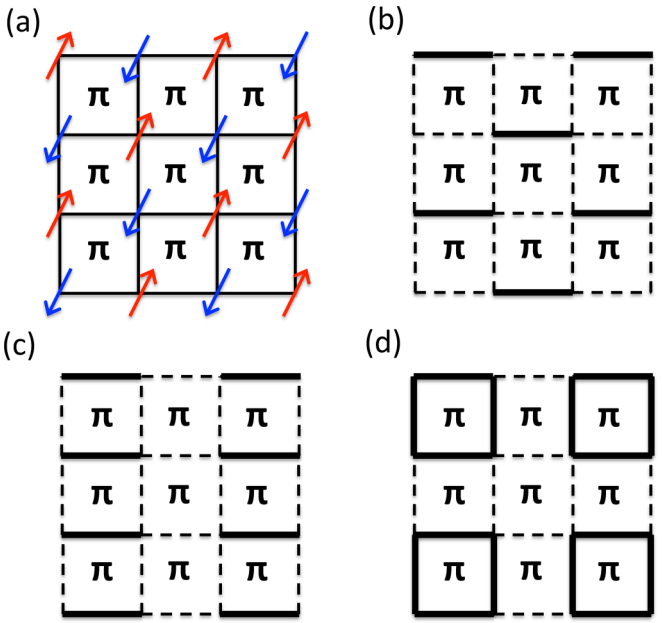

FIG. 4. Possible configurations of ordering: (a) AF order; (b) staggered VBS order; (c) columnar VBS order; (d) plaquette VBS order.

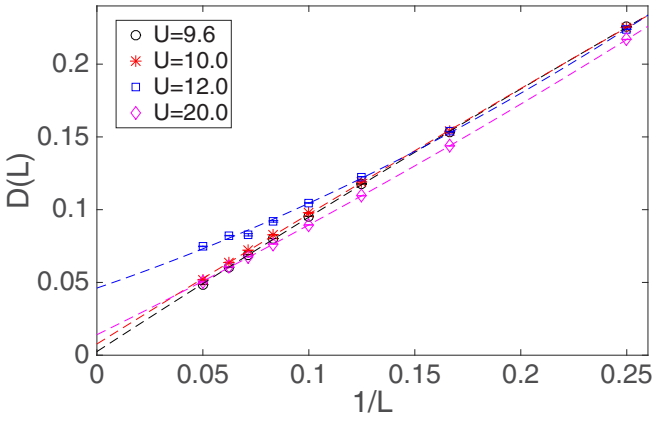

FIG. 5. Finite-size scalings of $D(L)$ vs $1/L$ as U varies in the π-flux $SU(4)$ Hubbard model. The quadratic polynomial fitting is used. Error bars are smaller than symbols.

directions are defined as

$$\chi_x(L,\vec{q}_{x_0}) = \frac{1}{L^4}\sum_{ij} d_{i,\hat{e}_x} d_{j,\hat{e}_x} e^{i\vec{q}_x\cdot\vec{r}},$$

$$\chi_y(L,\vec{q}_{y_0}) = \frac{1}{L^4}\sum_{ij} d_{i,\hat{e}_y} d_{j,\hat{e}_y} e^{i\vec{q}_y\cdot\vec{r}}, \tag{7}$$

where $\vec{q}_x = (\pi,0)$, $\vec{q}_y = (0,\pi)$, and $\vec{r}$ is the relative vector between sites i and j. The strength of the VBS order parameter is thus expressed as

$$D = \lim_{L\to+\infty}\sqrt{\chi_x(L,\vec{q}_{x_0}) + \chi_y(L,\vec{q}_{y_0})}. \tag{8}$$

In principle, the probability distribution of χ_x and χ_y can be used to further distinguish the cVBS and pVBS ordering on a square lattice. They exhibit different Z_4 symmetry-breaking patterns: For the cVBS ordering, the peaks of $P(\chi_x,\chi_y)$ are located at the angles of $0,\frac{\pi}{2},\pi,\frac{3\pi}{2}$, while for the pVBS ordering, its peaks are located at the direction of $\frac{\pi}{4},\frac{3\pi}{4},\frac{5\pi}{4},\frac{7\pi}{4}$. However, given the lattice size studied in our simulations, it is hard to distinguish the cVBS and pVBS orders by $P(\chi_x,\chi_y)$.

In Fig. 5, the finite-size scalings of the VBS order $D(L)$ are presented. With the Mott gap opening, the long-range VBS order starts to appear at around $U/t \approx 9$. In the next section, the phase-transition point is to be determined more accurately by calculating the Binder ratios. Due to the suppression of the overall kinetic energy scale, the U dependence of VBS order is nonmonotonic [37]. Moreover, this nonmonotonic behavior cannot be regarded as a signal of the suppression of VBS order by other competing orders.

IV. NATURE OF THE MOTT TRANSITION

Recently, large-scale PQMC simulations have been widely employed to investigate critical phenomena of a lattice model. For example, the spinless Dirac fermions on honeycomb and π-flux square lattices undergo a quantum phase transition to the charge-density-wave (CDW) order with increasing nearest-neighboring repulsion V [52–54]. This semimetal-CDW transition belongs to the chiral Ising universality class due to the fact that CDW ordering breaks the discrete sublattice symmetry [52]. In both the $SU(2)$ honeycomb-lattice and the $SU(2)$ π-flux square-lattice Hubbard models, increasing U triggers the semimetal-AF phase transition, which belongs to the chiral Heisenberg universality class [34,35]. However, the Mott transitions of the $SU(4)$ Dirac fermions are different on the honeycomb lattice and the π-flux square lattice. In both models, with increasing Hubbard U, the $SU(4)$ Dirac fermions undergo a semimetal-VBS phase transition. The Mott transition breaks the Z_3 symmetry on a honeycomb lattice [37], while the Z_4 symmetry is broken on a π-flux square lattice.

On the honeycomb lattice, the analytic part of the Ginzburg-Landau (GL) free energy contains a cubic term allowed by the Z_3 symmetry. Hence, generally speaking, the semimetal-VBS phase transition on a honeycomb lattice should be of first order [37,55]. However, the coupling of VBS to Dirac fermions can soften the phase transition to second order [37–41]. On a square lattice with a π flux, the VBS order breaks the Z_4 symmetry, and consequently the cubic term is not allowed in the analytic part of the GL free energy. Along the same lines as Ref. [37], we can evaluate the nonanalytic part of the GL free energy by tracing out the degrees of freedom of $SU(2N)$ Dirac fermions. At the mean-field level, the free-energy density that may contribute the cubic term at half filling is

$$f \approx -\frac{1}{\beta}\int_0^\Lambda \frac{d^2\vec{k}}{(2\pi)^2}\ln[(1+e^{\beta E_k})(1+e^{-\beta E_k})]^{4N}, \tag{9}$$

where $E_k = \sqrt{v^2k^2+|\psi|^2}$ is the single-particle spectrum around each Dirac cone, and $|\psi|$ is the gap function of the VBS order at the mean-field level; β is the inverse temperature, and Λ is the momentum cutoff. In the low-temperature limit, we have

$$\begin{aligned}\lim_{\beta\to\infty} f &= -4N\int_0^\Lambda \frac{dk_x dk_y}{4\pi^2}\sqrt{v^2k^2+|\psi|^2} \\ &= -\frac{2N}{3\pi v^2}[(\Lambda^2v^2+|\psi|^2)^{3/2}-|\psi|^3].\end{aligned} \tag{10}$$

We perform the Taylor expansion of the right-hand side of this equation at the critical point where $|\psi|\to 0$, and then we find a nonanalytic cubic term below

$$f_{\text{cubic}} = \frac{2N}{3\pi v^2}|\psi|^3 > 0. \tag{11}$$

This implies that the semimetal-VBS phase transition on a π-flux square lattice should be of second-order. This type of quantum phase transition can be investigated by the finite-size scalings of the numerical data.

To locate the phase-transition point more accurately, we define the Binder ratios as follows [34,38,56]: For χ_x, we define $\vec{q}_x = (\pi,0)$, $\vec{q}_{x_1} = (\pi+\frac{2\pi}{L},0)$, and $\vec{q}_{x_2} = (\pi,\frac{2\pi}{L})$. Then we have the binder ratios parallel and perpendicular to the x bonds on the $L\times L$ lattice,

$$B_1^x(L) = \frac{\chi_x(L,\vec{q}_x)}{\chi_x(L,\vec{q}_{x_1})},\quad B_2^x(L) = \frac{\chi_x(L,\vec{q}_x)}{\chi_x(L,\vec{q}_{x_2})}. \tag{12}$$

Similarly for χ_y, we define $\vec{q}_y = (0,\pi)$, $\vec{q}_{y_1} = (\frac{2\pi}{L},\pi)$, and $\vec{q}_{y_2} = (0,\pi+\frac{2\pi}{L})$. Then we have the Binder ratios

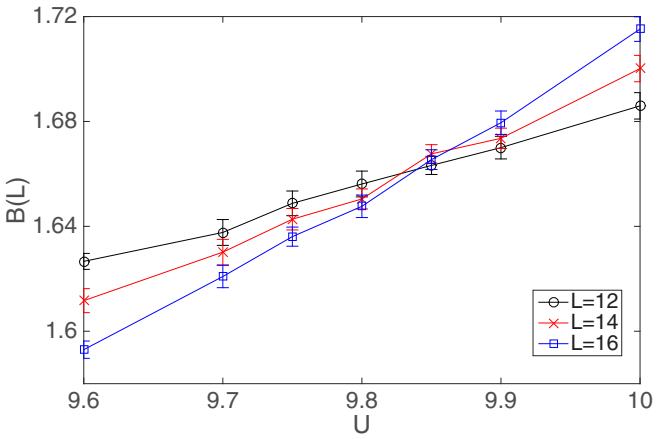

FIG. 6. Binder ratios $B(L)$ for the semimetal-VBS transition with different U and L. The crossing point suggests a critical value in between $U = 9.8$ and 9.9.

perpendicular and parallel to the y bonds on the $L\times L$ lattice,

$$B_1^y(L) = \frac{\chi_y(L,\vec{q}_y)}{\chi_y(L,\vec{q}_{y_1})}, \quad B_2^y(L) = \frac{\chi_y(L,\vec{q}_y)}{\chi_y(L,\vec{q}_{y_2})}. \tag{13}$$

At the critical point of the second-order phase transition, the Binder ratio should reach a size-independent value as the lattice size L grows. According to this principle, the critical coupling U_c can be determined in Fig. 6, where $B(L) = \frac{1}{4}[B_1^x(L) + B_2^x(L) + B_1^y(L) + B_2^y(L)]$ is an arithmetic average. The crossing point in Fig. 6 indicates a second-order phase transition with a critical coupling in between $U = 9.8$ and 9.9. Then we assume the VBS order obeys the following scaling ansatz [57–59]:

$$D^2(L) = L^{-z-\eta}\mathcal{F}[(U - U_c)L^{1/\nu}], \tag{14}$$

where η and ν are dimensionless critical exponents, z is the dynamic exponent, and $\mathcal{F}$ is the scaling function. As shown in Fig. 7, the critical exponent η can be extracted from the slope of the log-log plot of the $D^2(L)$-L curve in the critical region $U = 9.8$–9.9. η is found to be 0.86 ± 0.04 via the linear fitting with the assumption of $z = 1$. Due to the limitation of the lattice size that we can simulate, the critical exponent of ν cannot be extracted by data collapse.

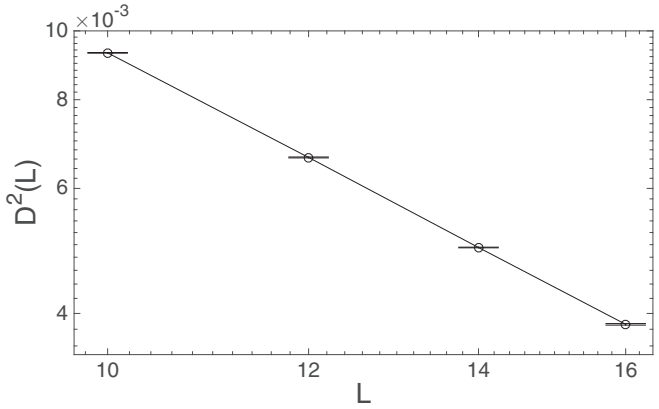

FIG. 7. Critical scaling behavior of the VBS order parameter $D^2(L)$ vs the lattice size L at $U/t = 9.8$. The critical exponent $z + \eta$ can be extracted from the slope of the log-log plot of the $D^2(L)$-L curve.

V. THE RING-EXCHANGE PROCESS

The above QMC results show the semimetal to the VBS transition in the π-flux $SU(4)$ Hubbard model on a square lattice, and the absence of AF ordering even at $U/t = 20$. In contrast, it has been shown in the previous work that the ground state of the zero-flux $SU(4)$ Hubbard model on a square lattice is associated with the AF order [36], which depends on U nonmonotonically. Until now, physics in the large-U limit for both the zero-flux and π-flux half-filled $SU(4)$ Hubbard models on a square lattice is still an open question.

In fact, in the strong-coupling regime, both the zero-flux and π-flux $SU(4)$ Hubbard models, to the second-order perturbation, identically reduce to the $SU(4)$ Heisenberg model with the single column self-conjugate representation. The differences between the zero-flux and π-flux Hubbard models arise from the higher-order perturbation terms, for example the next higher-order contributions from the four-site ring-exchange term.

The four-site ring-exchange terms can be expressed as follows:

$$H'^{(4)}(\square) = -\frac{1}{U^3}T_{-1}T_0T_0T_{+1} - \frac{1}{2U^3}T_{-1}T_{-1}T_{+1}T_{+1}, \tag{15}$$

where T_m corresponds to the hopping process that changes the interaction energy by mU. For the $SU(4)$ case, $m = -3$ to 3. (See Appendix for details.) In the four-site ring-exchange process, fermions hop along a linked loop in a plaquette. Unlike the zero-flux case, fermions in the π-flux model gain an additional π phase once they experience the ring-exchange process. As a result, the four-site ring-exchange terms of the zero-flux and π-flux models have opposite signs.

We speculate that the different four-site ring-exchange terms are responsible for the different orderings in the Mott-insulating phase in the strong-coupling regime. Previous QMC simulations of the $SU(4)$ Heisenberg model with the single-column self-conjugate representation on a square lattice show evidence of a gapless spin liquid. It would be interesting to check if the $SU(4)$ Heisenberg model is critical. If that is the case, then it will be reasonable to speculate that the four-site ring-exchange terms stabilize orderings of VBS and AF in the π-flux and zero-flux cases, respectively, depending on the signs of the ring-exchange terms.

VI. CONCLUSIONS AND DISCUSSIONS

In summary, we have employed the PQMC simulations to study the ground-state properties of the π-flux square-lattice $SU(4)$ Hubbard model. At the critical coupling in between $U = 9.8$ and 9.9, the $SU(4)$ Dirac fermions on the square lattice undergo a Mott transition to the VBS, which breaks the Z_4 discrete symmetry. The GL free energy is free of the cubic term in its analytic part, while its nonanalytic part contains the term of $|\psi|^3$ with a positive coefficient, which implies that the semimetal-VBS transition is of second order. The nonperturbative PQMC simulations also prove the existence of a second-order phase transition with critical exponent $\eta = 0.86 \pm 0.04$.

Our work demonstrates that the combination of the $SU(4)$ symmetry and the π flux dramatically affects the quantum phase transitions on a square lattice. Compared with the π-flux $SU(2)$ and the zero-flux $SU(4)$ models, at the even stronger critical coupling U_c the π-flux $SU(4)$ model undergoes a Mott transition to a VBS order rather than an AF order. Due to Fermi surface nesting, the zero-flux $SU(4)$ model enters a Mott-insulating state at infinitesimal coupling. The multiple fermion components enhance the charge fluctuations, which increases the critical coupling for the emergence of a Mott insulator. In the presence of a π flux, stronger spin fluctuations entirely suppress the AF ordering, and instead the VBS order emerges in the $SU(4)$ Mott-insulating state. $SU(4)$ Dirac fermions on the square lattice energetically favor VBS order rather than the AF order in the strong-coupling regime, which is consistent with the behavior of $SU(2N)$ Dirac fermions studied on a honeycomb lattice [37]. To account for the effect of a π flux on the ordering in the strong-coupling regime, we analytically derive by perturbation theory the ring-exchange term, which is the leading-order term that can reflect the difference between the π-flux and zero-flux $SU(4)$ Hubbard models. The ring-exchange terms for the two cases differ by a minus sign. However, definitive proof of the physical consequence of the ring-exchange term requires further study.

ACKNOWLEDGMENTS

This work is financially supported by the National Natural Science Foundation of China under Grants No. 11729402, No. 11574238, and No. 11328403. Z.Z. and Y.W. are grateful for the award of scholarships funded by the China Scholarship Council (Files No. 201606270067 and No. 201706275082). C.W. is supported by the AFOSR FA9550-14-1-0168. This work made use of the facilities of Tianhe-2 at China's National Supercomputing Centre in Guangzhou. Z.Z. and Y.W. also acknowledge the support of the Supercomputing Center of Wuhan University.

APPENDIX: CANONICAL TRANSFORMATION OF THE $SU(4)$ HUBBARD HAMILTONIAN IN THE STRONG-COUPLING LIMIT

The original Hamiltonian Eq. (1) can be written in the form

$$H = \sum_{m=-3}^{3} T_m + V, \tag{A1}$$

where V is the interaction term

$$V = U \sum_i \sum_{\alpha\neq\beta} n_{i\alpha} n_{i\beta}, \tag{A2}$$

and T_m is associated with the hopping process that changes the interaction energy by mU. For the $SU(4)$ case, $m=-3, -2, -1, 0, 1, 2, 3$. T_m can be explicitly expressed in terms of the projection operator $P_i^\alpha(n)$ for site i below

$$P_i^\alpha(0) = \prod_{\beta\neq\alpha}(1-n_{i\beta}), \quad P_i^\alpha(1) = \sum_{\beta\neq\alpha}(n_{i\beta}) \prod_{\gamma\neq\alpha,\beta}(1-n_{i\gamma}),$$
$$P_i^\alpha(2) = \sum_{\beta\neq\alpha}(1-n_{i\beta}) \prod_{\gamma\neq\alpha,\beta}(n_{i\gamma}), \quad P_i^\alpha(3) = \prod_{\beta\neq\alpha}(n_{i\beta}). \tag{A3}$$

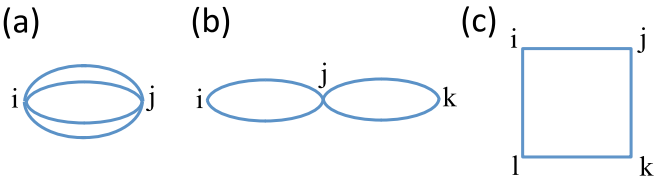

FIG. 8. The hopping process corresponding to the fourth-order perturbation term links (a) two, (b) three, or (c) four lattice sites.

Then the hopping terms are

$$T_{+3} = -\sum_{\langle i,j\rangle;\alpha} t_{ij}\left[P_i^\alpha(3) c_{i\alpha}^\dagger c_{j\alpha} P_j^\alpha(0)\right],$$
$$T_{+2} = -\sum_{\langle i,j\rangle;\alpha} t_{ij} \sum_{n=0}^{1}\left[P_i^\alpha(n+2) c_{i\alpha}^\dagger c_{j\alpha} P_j^\alpha(n)\right],$$
$$T_{+1} = -\sum_{\langle i,j\rangle;\alpha} t_{ij} \sum_{n=0}^{2}\left[P_i^\alpha(n+1) c_{i\alpha}^\dagger c_{j\alpha} P_j^\alpha(n)\right],$$
$$T_0 = -\sum_{\langle i,j\rangle;\alpha} t_{ij} \sum_{n=0}^{3}\left[P_i^\alpha(n) c_{i\alpha}^\dagger c_{j\alpha} P_j^\alpha(n)\right], \tag{A4}$$

and $T_{-m} = T_m^\dagger$.

In the strong-coupling limit of $|U/t| \to \infty$, the Hamiltonian can be block-diagonalized such that the interaction energy $\langle V\rangle$ is constant in each block with hopping processes serving as perturbations. For the block diagonalization of the Hamiltonian, a canonical transformation $H' = e^{iS} H e^{-iS}$ is performed to eliminate hopping between blocks associated with different $\langle V\rangle$ [60]. The perturbation terms can be formed as a product of hopping T_m's. The zeroth-order perturbation reads

$$H'^{(0)} = V + T_0. \tag{A5}$$

At half filling, the second- and fourth-order perturbations can be written as

$$H'^{(2)} = -\frac{1}{U} T_{-1} T_{+1}, \tag{A6}$$
$$H'^{(4)} = +\frac{1}{U^3} T_{-1} T_{+1} T_{-1} T_{+1} - \frac{1}{U^3} T_{-1} T_0 T_0 T_{+1} - \frac{1}{2U^3} T_{-1} T_{-1} T_{+1} T_{+1} - \frac{1}{3U^3} T_{-1} T_{-2} T_{+2} T_{+1} - \frac{1}{4U^3} T_{-1} T_{-3} T_{+3} T_{+1}. \tag{A7}$$

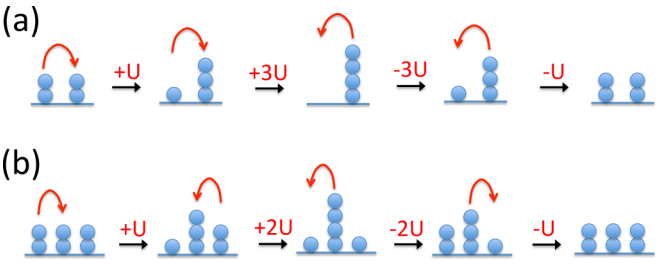

FIG. 9. (a) Hopping process $T_{-1}T_{-3}T_{+3}T_{+1}$ only occurs on two-site configurations. (b) Hopping process $T_{-1}T_{-2}T_{+2}T_{+1}$ only occurs on three-site configurations.

The second-order perturbation just involves the two-site hopping process, and it can be mapped to the $SU(4)$ Heisenberg model in the self-conjugate representation [61,62]. As shown in Fig. 8, the fourth-order perturbation corresponds to three different linked hopping processes, in which the hopping process $T_{-1}T_{-3}T_{+3}T_{+1}$ [Fig. 9(a)], $T_{-1}T_{-2}T_{+2}T_{+1}$ [Fig. 9(b)], and $T_{-1}T_{+1}T_{-1}T_{+1}$ do not describe the ring-exchange process on a four-site plaquette [Fig. 8(c)] [63]. Consequently, the ring-exchange process can be written as Eq. (15) in the main text.

[1] D. Jaksch and P. Zoller, New J. Phys. **5**, 56 (2003).
[2] J. Dalibard, F. Gerbier, G. Juzeliūnas, and P. Öhberg, Rev. Mod. Phys. **83**, 1523 (2011).
[3] N. Goldman, G. Juzeliūnas, P. Öhberg, and I. B. Spielman, Rep. Prog. Phys. **77**, 126401 (2014).
[4] E. Zohar, J. I. Cirac, and B. Reznik, Rep. Prog. Phys. **79**, 014401 (2015).
[5] H. Miyake, G. A. Siviloglou, C. J. Kennedy, W. C. Burton, and W. Ketterle, Phys. Rev. Lett. **111**, 185302 (2013).
[6] M. Aidelsburger, M. Atala, M. Lohse, J. T. Barreiro, B. Paredes, and I. Bloch, Phys. Rev. Lett. **111**, 185301 (2013).
[7] C. Wu, J. P. Hu, and S. C. Zhang, Phys. Rev. Lett. **91**, 186402 (2003).
[8] C. Honerkamp and W. Hofstetter, Phys. Rev. Lett. **92**, 170403 (2004).
[9] C. Wu, Phys. Rev. Lett. **95**, 266404 (2005).
[10] C. Wu, Mod. Phys. Lett. B **20**, 1707 (2006).
[11] A. V. Gorshkov, M. Hermele, V. Gurarie, C. Xu, P. S. Julienne, J. Ye, P. Zoller, E. Demler, M. D. Lukin, and A. M. Rey, Nat. Phys. **6**, 289 (2010).
[12] S. Taie, Y. Takasu, S. Sugawa, R. Yamazaki, T. Tsujimoto, R. Murakami, and Y. Takahashi, Phys. Rev. Lett. **105**, 190401 (2010).
[13] B. J. DeSalvo, M. Yan, P. G. Mickelson, Y. N. Martinez de Escobar, and T. C. Killian, Phys. Rev. Lett. **105**, 030402 (2010).
[14] S. Taie, R. Yamazaki, S. Sugawa, and Y. Takahashi, Nat. Phys. **8**, 825 (2012).
[15] G. Pagano, M. Mancini, G. Cappellini, P. Lombardi, F. Schäfer, H. Hu, X.-J. Liu, J. Catani, C. Sias, M. Inguscio, and L. Fallani, Nat. Phys. **10**, 198 (2014).
[16] C. Hofrichter, L. Riegger, F. Scazza, M. Höfer, D. R. Fernandes, I. Bloch, and S. Fölling, Phys. Rev. X **6**, 021030 (2016).
[17] G. Chen, K. R. A. Hazzard, A. M. Rey, and M. Hermele, Phys. Rev. A **93**, 061601 (2016).
[18] M. Hermele, V. Gurarie, and A. M. Rey, Phys. Rev. Lett. **103**, 135301 (2009).
[19] M. Hermele and V. Gurarie, Phys. Rev. B **84**, 174441 (2011).
[20] P. Nataf, M. Lajkó, A. Wietek, K. Penc, F. Mila, and A. M. Läuchli, Phys. Rev. Lett. **117**, 167202 (2016).
[21] I. Affleck, Phys. Rev. Lett. **54**, 966 (1985).
[22] D. P. Arovas and A. Auerbach, Phys. Rev. B **38**, 316 (1988).
[23] I. Affleck and J. B. Marston, Phys. Rev. B **37**, 3774 (1988).
[24] N. Read and S. Sachdev, Nucl. Phys. B **316**, 609 (1989).
[25] K. Harada, N. Kawashima, and M. Troyer, Phys. Rev. Lett. **90**, 117203 (2003).
[26] N. Kawashima and Y. Tanabe, Phys. Rev. Lett. **98**, 057202 (2007).
[27] K. S. D. Beach, F. Alet, M. Mambrini, and S. Capponi, Phys. Rev. B **80**, 184401 (2009).
[28] R. K. Kaul and A. W. Sandvik, Phys. Rev. Lett. **108**, 137201 (2012).
[29] A. Paramekanti and J. B. Marston, J. Phys.: Condens. Matter **19**, 125215 (2007).
[30] F. F. Assaad, Phys. Rev. B **71**, 075103 (2005).
[31] Y. Otsuka and Y. Hatsugai, Phys. Rev. B **65**, 073101 (2002).
[32] C.-C. Chang and R. T. Scalettar, Phys. Rev. Lett. **109**, 026404 (2012).
[33] Y. Otsuka, S. Yunoki, and S. Sorella, *Proceedings of the International Conference on Strongly Correlated Electron Systems (SCES2013)* (The Physical Society of Japan, Tokyo, 2013).
[34] F. Parisen Toldin, M. Hohenadler, F. F. Assaad, and I. F. Herbut, Phys. Rev. B **91**, 165108 (2015).
[35] Y. Otsuka, S. Yunoki, and S. Sorella, Phys. Rev. X **6**, 011029 (2016).
[36] D. Wang, Y. Li, Z. Cai, Z. Zhou, Y. Wang, and C. Wu, Phys. Rev. Lett. **112**, 156403 (2014).
[37] Z. Zhou, D. Wang, Z. Y. Meng, Y. Wang, and C. Wu, Phys. Rev. B **93**, 245157 (2016).
[38] Z.-X. Li, Y.-F. Jiang, S.-K. Jian, and H. Yao, Nat. Commun. **8**, 314 (2017).
[39] S.-K. Jian and H. Yao, Phys. Rev. B **96**, 195162 (2017).
[40] M. M. Scherer and I. F. Herbut, Phys. Rev. B **94**, 205136 (2016).
[41] L. Classen, I. F. Herbut, and M. M. Scherer, Phys. Rev. B **96**, 115132 (2017).
[42] R. Blankenbecler, D. J. Scalapino, and R. L. Sugar, Phys. Rev. D **24**, 2278 (1981).
[43] J. E. Hirsch, Phys. Rev. B **31**, 4403 (1985).
[44] F. Assaad and H. Evertz, in *Computational Many-Particle Physics*, Lecture Notes in Physics Vol. 739 (Springer, Berlin, 2008), p. 277.
[45] C. Wu and S. C. Zhang, Phys. Rev. B **71**, 155115 (2005).
[46] L. Wang, Y.-H. Liu, M. Iazzi, M. Troyer, and G. Harcos, Phys. Rev. Lett. **115**, 250601 (2015).
[47] Z. C. Wei, C. Wu, Y. Li, S. Zhang, and T. Xiang, Phys. Rev. Lett. **116**, 250601 (2016).
[48] Z.-X. Li, Y.-F. Jiang, and H. Yao, Phys. Rev. Lett. **117**, 267002 (2016).
[49] Z. Zhou, Z. Cai, C. Wu, and Y. Wang, Phys. Rev. B **90**, 235139 (2014).
[50] D. Ixert, F. F. Assaad, and K. P. Schmidt, Phys. Rev. B **90**, 195133 (2014).
[51] A. W. Sandvik, AIP Conf. Proc. **1297**, 135 (2010).
[52] L. Wang, P. Corboz, and M. Troyer, New J. Phys. **16**, 103008 (2014).
[53] Z.-X. Li, Y.-F. Jiang, and H. Yao, Phys. Rev. B **91**, 241117 (2015).
[54] Z.-X. Li, Y.-F. Jiang, and H. Yao, New J. Phys. **17**, 085003 (2015).
[55] J. Motruk, A. G. Grushin, F. de Juan, and F. Pollmann, Phys. Rev. B **92**, 085147 (2015).

[56] Y. Tomita and Y. Okabe, Phys. Rev. B **66**, 180401 (2002).
[57] J. Cardy, *Finite-size Scaling* (Elsevier, Amsterdam, 2012), Vol. 2.
[58] M. Campostrini, A. Pelissetto, and E. Vicari, Phys. Rev. B **89**, 094516 (2014).
[59] O. Melchert, arXiv:0910.5403.
[60] A. H. MacDonald, S. M. Girvin, and D. Yoshioka, Phys. Rev. B **37**, 9753 (1988).
[61] F. H. Kim, K. Penc, P. Nataf, and F. Mila, Phys. Rev. B **96**, 205142 (2017).
[62] S. Xu, J. Barreiro, Y. Wang, and C. Wu, arXiv:1707.01463.
[63] M. Takahashi, J. Phys. C **10**, 1289 (1977).